Microscale flow propulsion through bioinspired and magnetically actuated artificial cilia

Chia-Yuan Chen,[a] Ling-Ying Cheng, Chun-Chieh Hsu, and Karthick Mani
Department of Mechanical Engineering, National Cheng Kung University, Tainan 701, Taiwan

(Received 26 March 2015; accepted 11 May 2015; published online 22 May 2015)

Recent advances in microscale flow propulsion through bioinspired artificial cilia provide a promising alternative for lab-on-a-chip applications. However, the ability of actuating artificial cilia to achieve a time-dependent local flow control with high accuracy together with the elegance of full integration into the biocompatible microfluidic platforms remains remote. Driven by this motive, the current work has constructed a series of artificial cilia inside a microchannel to facilitate the time-dependent flow propulsion through artificial cilia actuation with high-speed (>40 Hz) circular beating behavior. The generated flow was quantified using micro-particle image velocimetry and particle tracking with instantaneous net flow velocity of up to 10^1 μm/s. Induced flow patterns caused by the tilted conical motion of artificial cilia constitutes efficient fluid propulsion at microscale. This flow phenomenon was further measured and illustrated by examining the induced flow behavior across the depth of the microchannel to provide a global view of the underlying flow propulsion mechanism. The presented analytic paradigms and substantial flow evidence present novel insights into the area of flow manipulation at microscale. © *2015 AIP Publishing LLC*. [http://dx.doi.org/10.1063/1.4921427]

I. INTRODUCTION

Cilia can be viewed as small hairs or flexible rods with a typical length between 2 and 15 μm covering the outer surface of microorganisms, such as paramecia, for effective flow generation.[1] Cilia can function as a flow actuator in many biological systems. For example, the left–right asymmetry pattern of a mouse embryo can be established by nodal flow through a vortical motion of cilia.[2] Cilia covering the fallopian tubes of females can move the fertilized ovum from the ovary to the uterus, as well as sweep mucus and dirt out of the airway in human lungs and trachea to prevent infections.[1] Ependymal cilia in humans can also generate a laminar flow of cerebrospinal fluid through the cerebral aqueduct to avoid hydrocephalus formation.[3] The physical concept behind these flow propulsion phenomena was further illustrated using the Scallop theorem. Generally, a scallop can slowly open then quickly close its shell to squirt out water; however, such kinematic behavior in a low Reynolds flow regime is not beneficial because only the reciprocal motion can be performed from such behavior. Therefore, a nonreciprocal motion was suggested for efficient flow manipulation at microscale.[4] This motion was observed in the cilia's motion, in which two distinct trajectories were followed for the power and recovery strokes in one beating cycle of cilia. A previous investigation also indicated that a metachronal wave is created in the epithelium,[5] wherein the collective movement of cilia moves in a concerted fashion. This wavy motion is characterized by sequential out-of-phase beating behavior between any two adjacent cilia and can be identified as either antiplectic or symplectic metachronism depending on the directions of the wave propagation and the generated fluid velocity through cilia actuation.[1] The synergic effect of these motion dynamics is very effective

[a]Author to whom correspondence should be addressed. Electronic mail: chiayuac@mail.ncku.edu.tw

as the swimming speed of a paramecium can reach up to 1 mm/s, which results from the collective beating of thousands of cilia covered on its surface.

Recently, the use of artificial cilia for microscale flow manipulation with systematic investigation has only engendered speculation. One of the pioneers that generated substantial flows at microscale through artificial cilia actuation was reported in the literature.[6] An electrostatic force was applied to drive the motion of artificial cilia, and the generated local mean fluid velocity was $>500\,\mu$m/s at the operation frequency of up to 200 Hz. However, the potential applications of the presented system remain limited as electrolysis may occur during the electrostatic actuation, in addition to the possibly detrimental effects on biological components caused by the applied high electrical field. As an alternative to achieve a better flow control for microfluidic applications, several paradigms based on the concept of magnetically actuated artificial cilia have aroused research interest for successful demonstration.[7–13] First, a self-assembly process was performed to fabricate a series of magnetized artificial cilia by using a superparamagnetic bead with a diameter of $4.4\,\mu$m.[9] A tilted conical motion was conducted by controlling the tilting angle of the artificial cilia under the alteration of the applied magnetic field. Typically, the generated fluid velocity is in the order of few micrometers per second. Additional alternatives for various motion controls of magnetic artificial cilia were also achieved using an external rotating magnet.[7,8,10] However, this magnetic field control method may be hindered if a higher degree of magnetic field orientation control is in need. Aside from the flow propulsion application, these artificial cilia are also beneficial in microscale flow regimes, in which mixing is an issue because of the low efficient diffusion of the fluids at microscale.[14–16] In these studies, the influences of the trajectories of artificial cilia on the induced vortical flow structures were resolved and discussed from both the experimental and numerical perspectives. A planar asymmetric beating behavior of an artificial cilium can generate out-of-plane vortices inside a microchannel, which are advantageous to assist the molecular diffusion between two fluids in a micromixing task.[16] Such flow-diverting technique to generate vortical flow structures also sheds light on future development of cell culture environment by using microfluidics, in which controlling the local fluid distribution for cell responses under various applied flow-induced mechanical stresses is necessary. Additionally, light-actuated artificial cilia, which rely on the actuation of artificial cilia by using specific light sources with different wavelengths, provide novel insights into the remote control of artificial cilia.[17] Although this method seems promising, future applications are limited because of its sophisticated process for artificial cilia fabrication and integration. In short, magnetically actuated artificial cilia cause no electrolysis and have less negative effects on biological components with capabilities of easy integration into a microfluidic platform (if the required magnetic coils can be reduced in size). Thus, these artificial cilia should be treated as a promising alternative for microscale flow control.

A time-reversible flow control using microfluidics is pivotal for hemodynamic-related applications. Hemodynamics in microcirculation is important to the etiology of hemorheology and circulatory diseases.[18,19] In microvessels with diameters below $200\,\mu$m, the assumption of homogeneous continuum is no longer valid, and the rheological properties of individual red blood cell (RBC) become relevant to the physiology and pathologies of the microcirculatory system.[20] The transient dynamics of RBCs are predominantly affected by the shear stress in the flow.[18] Under the influence of a shear flow applied by the local and systematic disturbances of hemostasis, RBCs can present various dynamic states, such as steady tank-treading, swinging, unsteady tumbling, and chaotic motion, which may lead to detrimental effects on the blood circulation.[18] The influences of these changes in RBC orientation and deformation give rise to additional concerns regarding the design of a micro total analysis system, in which the hemodynamics of individual RBC should be evaluated and assessed in a microfluidic platform for early detection of pathological flow symptoms in the blood flow.[21] Recent studies also indicated that in the inner lining of a blood vessel wall, endothelial cells play an important role in regulating downstream intracellular responses and modulating the gene/protein expression pathway through the conversion of the wall shear stress load to biochemical signals.[22–25] Specifically, one of the major findings from the perspective of fluid dynamics concluded that the human aortic endothelial cells are more inclined to proliferate in an oscillatory flow rather than an

unidirectional laminar one.[22] Therefore, a microfluidic device, which can periodically generate a time-dependent/reversible flow in addition to a uniform flow, is practically advantageous for RBC-related assessments performed on a portable chip. Driven by this motive, the current work aims to develop a micropumping platform that utilizes artificial cilia for oscillatory flow generation. In addition, based on previous published concepts using artificial cilia with similar magnetic field control system for micromixing applications,[14–16] the presented artificial cilia method is believed to be a robust and reliable microscale flow manipulator that facilitates both flow propulsion and mixing functions on a single portable chip and is highly demanded for microfluidic applications.

II. MATERIAL AND METHODS

The microchannel with the artificial cilia embedded for flow propulsion was manufactured through a series of micro-milling and micro-casting processes steps. These steps are illustrated in Fig. 1. First, the microchannel layout was designed to incorporate two types of microchannel regions, namely, zones with and without artificial cilia. The zone with artificial cilia (labelled as zones A and B) provided a thrust force for flow propulsion applications, and the zone without artificial cilia was prepared to test biomolecules, such as RBCs or cells of interest under various flow stresses wherein the driving force was directly induced from the zone with artificial cilia. The dimensions and fabrication procedures of these two zones are illustrated in Figs. 1(a) and 1(b), respectively. The substrate is acrylic with 5 mm in thickness. The zones and artificial cilia were structured by micro-milling to obtain the desired patterns. Specifically, the acrylic substrate was engraved to define the geometry of the microchannel serving as a mold for the follow-up casting process. In the zones with artificial cilia, each of the microholes with 50 μm diameters and 400 μm depths was drilled to define the geometrical features of each

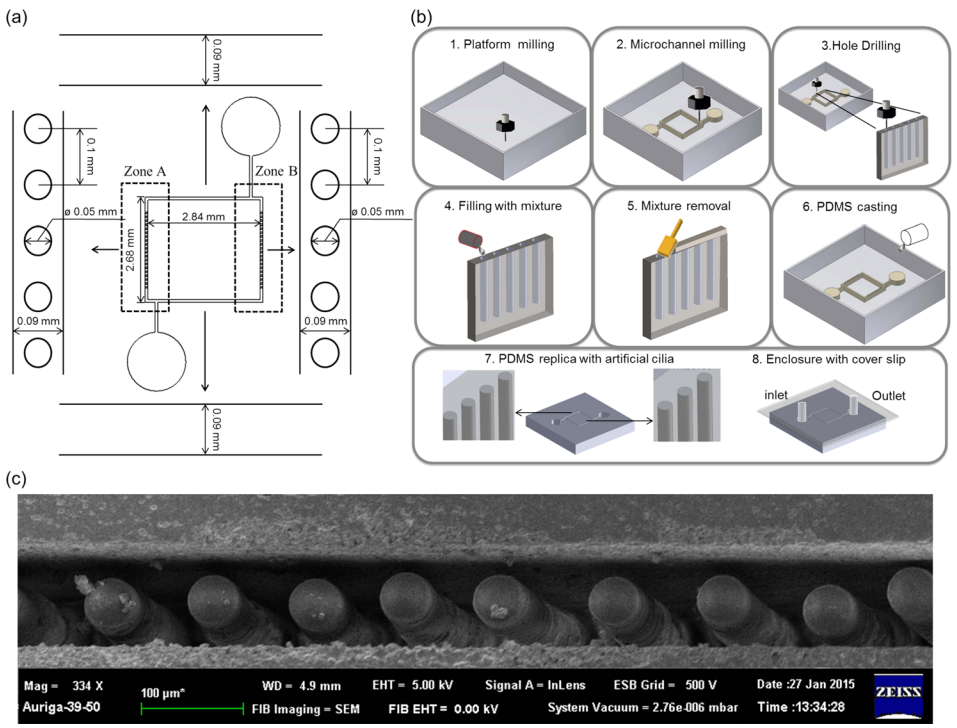

FIG. 1. Schematic of microchannel layout, fabrication process flow, and fabricated artificial cilia. (a) Dimensions of the microchannel and artificial cilia holes. (b) An acrylic substrate was first carved to define the geometry of the microchannel through micromilling and microdrilling (panels 1–3). Subsequently, the holes were filled with the mixture of polydimethylsiloxane (PDMS) solution and magnetic particles (panels 4 and 5). PDMS casting (panels 6 and 7) and microchannel enclosure through oxygen plasma surface treatment (panel 8). (c) Scanning electron microscope graph of the fabricated microchannel with artificial cilia protrusion from the microchannel bottom. Each artificial cilium is 50 μm in diameter.

artificial cilium. The major idea in the determination of the artificial cilia dimensions is to enable a high degree of moving capability by increasing the aspect ratio (depth/diameter) of the fabricated artificial cilia. However, such an increase in aspect ratio has to be compromised with the capability of the micro-casting process because the success rate of this process decreases with the increasing the aspect ratio of the artificial cilia. Therefore, considering this phenomenon, the value of the aspect ratio was decided to be eight in this work. Thereafter, these microholes were filled with artificial cilia composites. The artificial cilia composites were prepared from a mixture of commercially available 5 μm neodymium–iron–boron magnetic particles (MQP-15-7, Magnequench, Singapore) and PDMS solution (Sylgard 184, Dow Corning Corp., Midland, USA). The weight ratio of the particles to PDMS was 1:4. This value was selected by considering the tradeoff between the magnetic loading of the magnetic particles and the flexibility of the PDMS material. The increase of the amount of magnetic particles in the artificial cilia composite causes the increase of magnetic loading but decreases the flexibility of the artificial cilia. Decoupling the flexibility of the artificial cilia from their magnetic properties is difficult. In this regard, the ratio was selected as a substantial net flow was generated in this work. Once the filling of the microholes was completed, the entire mold was filled with degassed PDMS liquid solution, and it was followed by a curing process. This process involved hotplate baking at 95 °C for 48 h. A corresponding PDMS replica was then obtained after peeling the solidified PDMS material from the mold. Subsequently, the fabricated artificial cilia were magnetized to allow that the magnetic torque of the artificial cilia in a magnetic field was efficient. Finally, the microchannel openings were enclosed through oxygen plasma treatment. This method was successfully performed for the fabrication of an active micromixer.[14] However, the fabrication process in the present work was modified to fabricate the artificial cilia with higher aspect ratio (depth/diameter = 8) than those of the previously reported results (depth/diameter = 6) with the same cilium diameter (50 μm). As demonstrated in this work, such improvement enabled a better flow control in terms of flow propulsion.

To facilitate the artificial cilia actuation through magnetic force, a custom-built four-coil system was assembled by integrating a data acquisition device (NI cDAQ-9174, National Instruments, USA) and a computerized user command interface. The data acquisition device contained modules embedded for signal inputs and outputs (NI 9201 and 9264) and was connected to four magnetic coils (electromagnets). An external power supply (GPR-3510HD DC Power Supply, Instek, Taiwan) was also connected to the data acquisition device through a driving circuit to serve as an energy source for the actuation of artificial cilia. Each coil set consisted of an iron bar with a hexagonal cross section (1 cm on each side) wrapped with a single-strand 24-gauge magnetic coil at 1200 turns. The generated magnetic field can reach up to 0.08 T. By controlling the external magnetic field generated by the electromagnets, the artificial cilia were driven to perform a tilted conical motion. The time duration of the electrical current supplied to the coils for magnetic field generation was achieved with a modulated pulse-width modulation (PWM) waveform. The PWM switching frequency was set at 240 Hz to reduce the effect of hysteresis. The rotational movement of each artificial cilium was achieved by imposing a sinusoidal wave on each electromagnet. To provide information regarding the accuracy of the motion control of artificial cilia during propulsion, the relationship between the rotational frequency and the motion trajectory of the artificial cilia was quantified. This task was achieved through high-speed recording (NR4-S2, IDT, Tallahassee, FL, USA) with a frame rate of up to 1000 Hz. The kinematics of artificial cilia were also analyzed through DLT dataviewer2, a motion analysis software.[26]

The generated flow fields during artificial cilia propulsion in addition to the interaction between artificial cilia and surrounding fluid elements were quantified using micro-particle image velocimetry (μPIV), a flow visualization method. To conduct this flow measurement, 0.1% fluorescent polystyrene particles with diameter of 3.2 μm each (Microgenics, Inc., Fremont, CA, USA) were introduced into the microchannel via injection. Instantaneous particle motions over time were imaged using a fluorescent microscope (BX60, Olympus Corp., Japan). Commercially available PIV software (proVISION, IDT, Tallahassee, FL, USA) was used to process the acquired fluorescent particle images. An adaptive interrogation window method was

selected for velocity calculation with a spatial resolution of 6 μm. The presented μPIV calculation algorithm was validated by comparing the experimental and theoretical data with high agreement, which can be found in the literature.[15,27]

III. RESULTS

The time-dependent trajectories of artificial cilia during propulsion actuation were documented and compared with the corresponding circular fitting results at five selected triggering rotational frequencies (Fig. 2). Decreasing rotational radius of the artificial cilium was observed when the rotational frequency increased. The rotational radius exhibited the largest value (31.8 μm) at 10 Hz and reduced to 10.1 μm at 50 Hz linearly. By comparing the actual and fitted circular trajectories, the actual trajectory at 50 Hz was closer to a circular shape than that at 10 Hz and the degree of similarity decreased with decreasing rotational frequency. The relative large deviation between the actual and the fitted trajectories at low frequencies was primarily caused by the direct contact between the artificial cilium and the side wall. At such low rotational frequency, the rotational radius was increased, and the lateral displacement of the artificial cilium during cycling rotation was limited because of the narrow width of the microchannel (90 μm in our design). As a result, a skewed rotational trajectory (with relative long axis along the y-axis) was measured. This finding is consistent with those at the frequencies of 20 and 30 Hz. However, this result is opposite to the case of the artificial cilia at a higher frequency (50 Hz), where a more circular-shaped trajectory with the relative small rotational radius was observed. To identify the limits of the rotational frequency of artificial cilia, frequencies out of the presented rotational frequencies range (from 10 Hz to 50 Hz) were also tested. With a higher frequency (over 50 Hz) the rotational radius was still too small ($<$10 μm) and no net flow was generated. In the case of the low rotational frequency ($<$10 Hz) test, although the rotational radius was enlarged, the generated net flow was found insignificant. The major reason that contributed to this phenomenon lies in the lack of sustainable fluid elements that can be induced with such extremely low rotational frequency of artificial cilia. Therefore, the actuation frequency of 40 Hz was selected in this work as an optimized frequency value when the largest net flow was generated (as shown in the Results sections) compared with those at other frequencies

The presented flow propulsion method using artificial cilia was characterized through quantification of the generated peak flow velocity at three different rotational frequencies (30, 40, and 50 Hz). Both the generated forward and backward peak velocities during flow propulsion were recorded and measured over time at the frame rate of 200 Hz, and the net flow velocity results were measured with frame rates aligned to each corresponding rotational frequency. For

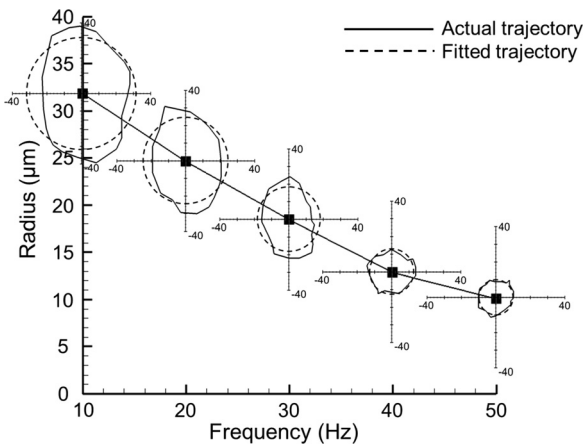

FIG. 2. Comparison of actual (solid line) and fitted (dashed line) circular trajectories of artificial cilia at five selected triggering frequencies. Fitted circle radius values at 10, 20, 30, 40, and 50 Hz are 31.8, 24.6, 18.4, 12.9, and 10.1 μm, respectively.

example, the frame rate of 30 Hz was selected when the rotational frequency was 30 Hz. With the synchronization of the rotational frequency and the image acquisition frame rate, the net flow velocity was clearly identified. The quantified results are shown in Fig. 3. The measurement of the induced flow speed by using these two types of frame rates implied that the generated flow with the current device is imperfectly uniform but involves slight oscillatory flow patterns. This physical flow behavior was primarily caused by the periodically rotational nature of each artificial cilium. The detailed underlying flow propulsion mechanism is presented in Sec. III (Results, paragraphs 5 and 6) through the evaluation of particle trajectories in the flow. By means of matching the rotational frequency and the frame rate, the induced oscillatory flow effect was eliminated; therefore, the primary flow propulsion elements were identified. Such information is beneficial to provide evidence regarding the concept of the presented flow propulsion method. Both the measured peak maximum and minimum velocity results are shown in the first column of Fig. 3, and the net flow results are presented in the second column.

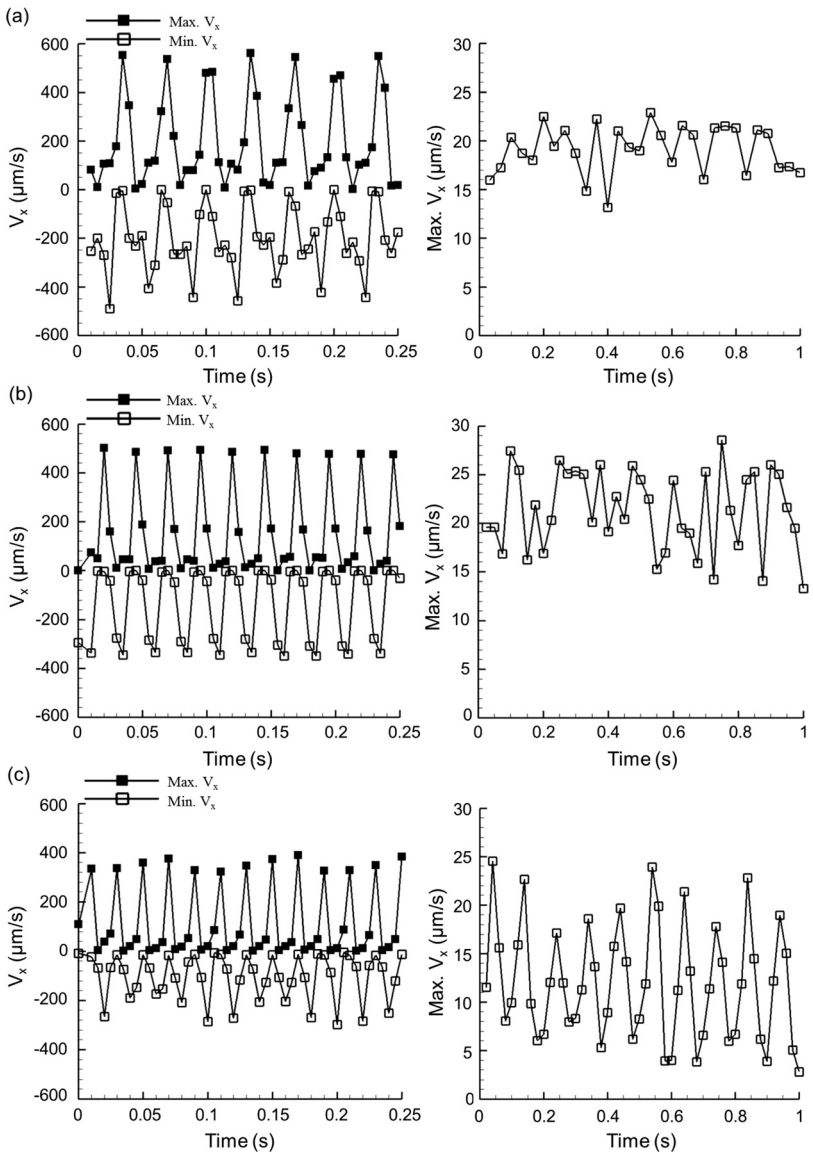

FIG. 3. Generated time-dependent streamwise peak flow velocity at the rotational frequencies of 30 (a), 40 (b), and 50 Hz (c). Particle images were recorded at a frame rate of 200 Hz (first column). In the second column, the frame rate was identical to the corresponding selected rotational frequency for quantification of the induced net flow.

Although the oscillatory flow behavior was significant in all three datasets (recorded at 30, 40, and 50 Hz), most of the absolute positive peak values were higher than the absolute negative peak values. This phenomenon is more pronounced from the datasets recorded with frame rates of 30 and 40 Hz. Hence, the flow was actually propelled going forward. The quantification of the induced net forward flow over time with three rotational frequencies is shown in the second column of Fig. 3, in which the highest positive flow peak over each 1 s time window (28.6 μm/s) existed at the rotational frequency of 40 Hz. Statistical results also showed that the average peak flow was the highest (21.4 μm/s) at 40 Hz. Therefore, an optimized rotational frequency of 40 Hz for artificial cilia actuation was selected in this work for further in-depth assessment.

To investigate the hydraulic propulsion phenomenon during the artificial cilia actuation, in-plane induced flow patterns were visualized and analyzed. Initially, ensemble streamwise velocity distribution on five selected planes in the zone without artificial cilia along the depth was quantified in Fig. 4(a). The induced flow was more significant on the plane of the cilium top (400 μm above the microchannel bottom) than those on the other planes. This characteristic is advantageous for local flow propulsion applications as the induced flow can be concentrated closely to an artificial cilia top region. Hence, artificial cilia with various depth values can be fabricated depending on the location where the local flow is necessary to be generated. To quantify the net generated velocity profiles through artificial cilia propulsion, the flow patterns were measured in the same region at the frame rate of 40 Hz (identical to the rotational frequency of artificial cilia) as shown in Fig. 4(b), and the corresponding flow profiles across the width of the zone without artificial cilia on five selected planes are also illustrated in Fig. 4(c). As previously mentioned, the generated flow is the most substantial and pronounced on the 400 μm plane (plane of artificial cilia top), which significantly decreases away from its depth. The generated net flow velocity was approximately 12.0 μm/s on average; this finding is over four times larger than those on other planes. A parabolic velocity profile across the width of the microchannel was also found on the plane of the artificial cilia top (Fig. 4(c)).

The demonstration of the time-reversible flow control is illustrated in Fig. 5 and in the video in the supplementary material.[28] Two datasets with frame rates of 200 (Fig. 5(a)) and 40 Hz (Fig. 5(b)) were collected at the same rotational frequency (40 Hz) of the artificial cilia. The total recording time for each data set is 10 s, and the artificial cilia were rotated clockwise during the first 3 s. This procedure is followed by a 7 s counterclockwise rotation. To depict the instantaneously induced flow behavior in a global perspective, the changes of the average maximum and minimum streamwise velocities along the microchannel centerline over a 1 s time window were plotted and compared. The peak velocity difference (max. V_x + min. V_x) decreased significantly (from 43.5 μm/s to −25.7 μm/s) after the initiation of the reverse rotational step (Fig. 5(a)). A similar trend can be found in Fig. 5(b), in which the peak net velocity difference steadily converged to about 12.6 μm/s over time during the reverse rotation of artificial cilia. The response time for this reversible flow control took <1 s for the induced flow to stop and flow toward the opposite direction. Given that this reversed flow control was achieved directly through the rapid motion control of artificial cilia and no mechanical component was

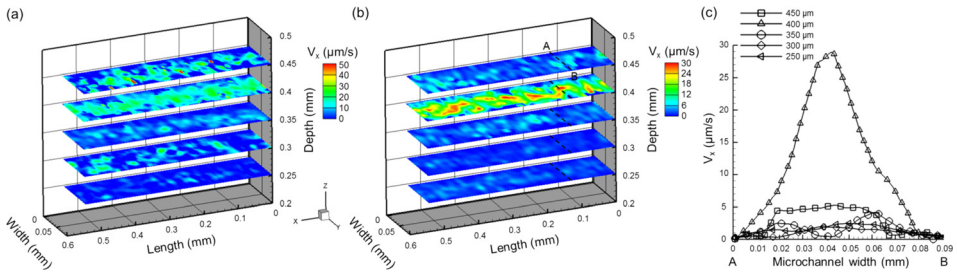

FIG. 4. Calculated ensemble streamwise velocity distribution ((a) and (b)) and extracted velocity profiles (c) on five measurement planes across the depth of the microchannel. Data were collected at frame rates of 200 (a) and 40 Hz (b) with rotational frequency of artificial cilia at 40 Hz for three cycles of rotation. (c) Corresponding velocity profiles across the width of the microchannel (along the AB dashed line).

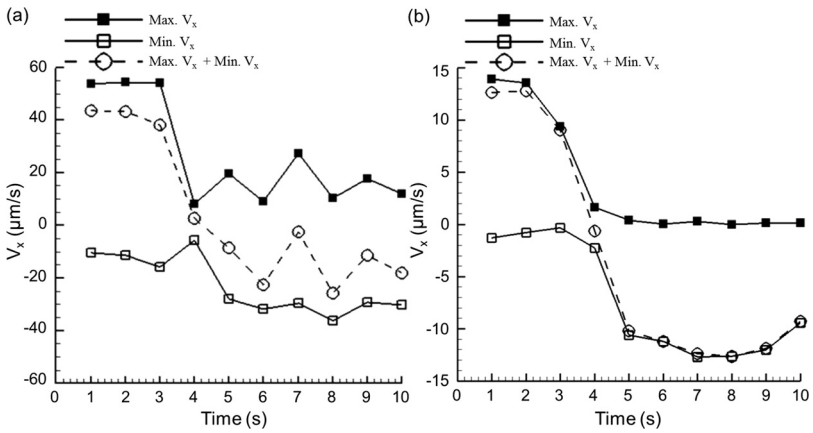

FIG. 5. Time-reversible control was achieved through the change of rotational direction of artificial cilia. Induced maximum and minimum flow velocity values along the microchannel centerline (at a depth of 400 μm above the microchannel bottom) were plotted over each 1 s time window at the recording frame rates of 200 (a) and 40 Hz (b). Rotational speed was 40 Hz with clockwise rotation in the first 3 s and counterclockwise rotation in the other time frames.

involved in the action mode, the presented method may likely replace traditional methods that utilize an infuse/withdraw syringe pump for a reverse flow control through mechanical components which are usually suffered by intrinsic hardware delay.

The underlying flow propulsion phenomenon was further analyzed via particle tracking method by investigating the mechanism by which a particle was propelled in the induced flow during the period of artificial cilia actuation. This information can shed light on future development for better flow manipulation at microscale in the field of microfluidics. As shown in Fig. 6(a), a particle was selected with delineated motion trajectory over time provided (shown in red solid line) to document the interaction between the rotating artificial cilium and the particle. Given that the particle motion was primarily caused by the induced flow from the movement of an artificial cilium, the relative artificial cilium trajectory was also identified and compared as highlighted with a white dashed line to clearly depict this phenomenon, in addition to the visualization of the particle trajectory. Based on particle dynamic behavior, three phases of action were identified: phases I, II, and III (Fig. 6(b)). In phase I, a significant back and forth motion behavior existed (Fig. 6(c)) with net forward displacement. This phase began when the cilium traveled from 0 T to 0.5 T. During this time window, the selected particle moved forward in the bottom left corner of the region of interest, while the artificial cilium went through a power stroke (moved from top to bottom ends) on the right hand side of this region. The positive axial velocity distribution on the right panel of Fig. 6(c) at the time point of 0.25 T supports this observation. Further investigation on the particle trajectory at later time stages shows that the particle moved backward during the time frames from 0.5 T to 0.75 T. In this case, the particle was repelled to move backward during the recovered stroke of the artificial cilium; the cilium moved from bottom left to the top left in the region of interest. This movement was expected in this time window. The artificial cilium moved to occupy the original resident space of the particle and then surpassed it. Therefore, the particle was forced to move backward because no space was available for the particle to move forward. Forward movement of the particle occurred again during the time window from 0.75 T to 1 T, in which the artificial cilium will finish one rotational cycle and was subjected to the next cycle of actuation. Consequently, the flow was forced to move forward with the accompanying particle to satisfy the continuity equation. This movement was evidenced by the corresponding velocity map, in which a positive velocity distribution was found in this region (Fig. 6(c); most right bottom subfigure).

Another forward movement of the particle existed with longer and consistent traveling distance when the artificial cilium moved in the time window from 2 T to 4 T (Fig. 6(d)). During this time period, the particle moved forward along the left side of the region of interest. Although the cycling motion, especially the recovery stroke portion of the artificial cilium

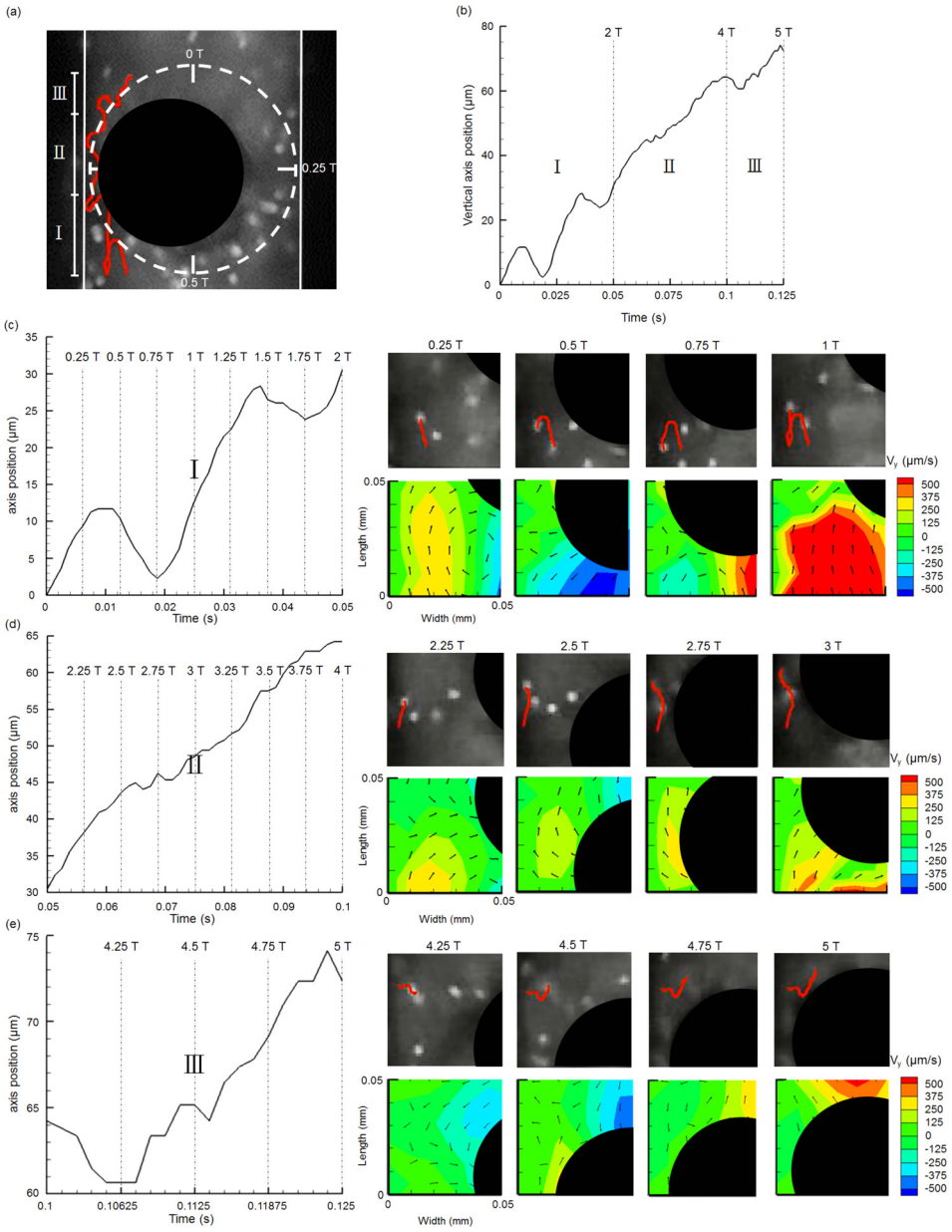

FIG. 6. Instantaneous particle tracking results with corresponding surrounding flow fields quantified through μPIV. (a) Illustration of induced particle trajectory (highlighted in red) with three phases of action under a cyclic rotational motion of an artificial cilium (dark circle). (b) Three phases of action of the particle's trajectory were identified showing the relationship between the axial position of particle and time. Time periods for phases I, II, and III are 0.05, 0.05, and 0.025 s, respectively, which also correspond to two, two, and one rotational cycles of the artificial cilium (with rotational frequency of 40 Hz), respectively. Axial positions of the particle over time were plotted (left panel) with surrounding axial velocity maps provided (right panel) in phases I (c), II (d), and III (e).

during rotation, turned the particle aside from its straight course, this influence was insignificantly relative to the forward movement of the particle. Evaluation of the associated velocity maps supported this observation, which implied that positive streamwise velocity distribution is more pronounced across the flow domain in this area. Taking one step further to track the particle motion after 4 T time point, an intermittent particle movement behavior existed (Fig. 6(e)). In this case, the particle approximately migrated out of the affected region of artificial cilium in motion. The additional influence of the induced flow from an adjacent artificial cilium began to influence the particle motion. The induced flow pattern in this area was quite complex, which

contributed to the diversely dynamic responses of the particle in terms of particle movement. However, the net forward movement of the particle can still be observed.

By means of the demonstrated results using flow visualization and particle tracking methods, the flow propulsion mechanism presented in this work was developed on the basis of a hydrodynamic benefit effect. This effect was accomplished through the orientation consistency between the titling and rotation directions of the artificial cilia, and is illustrated as the following. After the micro-casting process, all artificial cilia titled inwardly. Therefore, artificial cilia were tilted rightward in zone A and leftward in zone B. During the clockwise rotation of the artificial cilia, a net flow was generated in zone A with a direction moving toward the upstream of the entire device. Similarly, the other net flow was generated in zone B with a direction moving toward the downstream of the entire device. These two generated net flows were combined and constituted a strong net flow that circulated clockwise in the entire device. A consistent net flow behavior was found with opposite flowing direction when all artificial cilia rotated counterclockwise.

IV. CONCLUSIONS

Microscale flow propulsion was achieved with time-reversible flow control capability through artificial cilia actuation. The μPIV method, which provides quantitatively depth-wised flow patterns for flow assessment of the generated flow fields, was used to elucidate the underlying mechanism of flow propelling. The generated flow speed can reach 10^3 μm/s with net flow speed up to 10^1 μm/s. The generated flow field was mostly concentrated in the area close to the artificial cilia top plane, which is beneficial for local flow control. A parametric study was also conducted to identify the dominant factors that contributed to the effectiveness of the presented flow pumping concept. An optimized rotational frequency of 40 Hz for artificial cilia actuation was provided. This frequency generated a significant net forward flow for diverse microfluidic applications. Most importantly, the present flow propulsion concept using artificial cilia further extends the current practice of artificial cilia applications to multiple flow control options including micromixing and thrust generation, which serves as a better alternative for microscale flow manipulation.

ACKNOWLEDGMENTS

This study was supported through the Ministry of Science and Technology of Taiwan under Contract Nos. MOST 103-2221-E-006-269 and MOST 102-2221-E-006-297-MY3 (to Chia-Yuan Chen). This work would not be possible without the facility provided by Center for Micro/Nano Science and Technology, National Cheng Kung University. The research was, in part, supported by the Ministry of Education, Taiwan, Republic of China through the Aim for the Top University Project to the National Cheng Kung University (NCKU).

[1]J. M. J. d. Toonder and P. R. Onck, Trends Biotechnol. **31**, 85–91 (2013).
[2]S. Nonaka, H. Shiratori, Y. Saijoh, and H. Hamada, Nature **418**, 96–99 (2002).
[3]I. Ibanez-Tallon, A. Pagenstecher, M. Fliegauf, H. Olbrich, A. Kispert, U. P. Ketelsen, A. North, N. Heintz, and H. Omran, Hum. Mol. Genet. **13**, 2133–2141 (2004).
[4]E. M. Purcell, Am. J. Phys. **45**, 3–11 (1977).
[5]M. A. Sleigh, *Cilia and Flagella* (Elsevier Science & Technology Books, 1974).
[6]J. den Toonder, F. Bos, D. Broer, L. Filippini, M. Gillies, J. de Goede, T. Mol, M. Reijme, W. Talen, H. Wilderbeek, V. Khatavkar, and P. Anderson, Lab Chip **8**, 533–541 (2008).
[7]B. A. Evans, A. R. Shields, R. L. Carroll, S. Washburn, M. R. Falvo, and R. Superfine, Nano Lett. **7**, 1428–1434 (2007).
[8]A. R. Shields, B. L. Fiser, B. A. Evans, M. R. Falvo, S. Washburn, and R. Superfine, Proc. Natl. Acad. Sci. U.S.A. **107**, 15670–15675 (2010).
[9]M. Vilfan, A. Potocnik, B. Kavcic, N. Osterman, I. Poberaj, A. Vilfan, and D. Babic, Proc. Natl. Acad. Sci. U.S.A. **107**, 1844–1847 (2010).
[10]J. Belardi, N. Schorr, O. Prucker, and J. Ruhe, Adv. Funct. Mater. **21**, 3314–3320 (2011).
[11]G. Kokot, M. Vilfan, N. Osterman, A. Vilfan, B. Kavcic, I. Poberaj, and D. Babic, Biomicrofluidics **5**, 34103 (2011).
[12]S. N. Khaderi, J. M. J. den Toonder, and P. R. Onck, Biomicrofluidics **6**, 014106 (2012).
[13]P. J. Glazer, J. Leuven, H. An, S. G. Lemay, and E. Mendes, Adv. Funct. Mater. **23**, 2964–2970 (2013).
[14]C. Y. Chen, C. Y. Chen, C. Y. Lin, and Y. T. Hu, Lab Chip **13**, 2834–2839 (2013).
[15]C. Y. Chen, C. Y. Lin, and Y. T. Hu, Exp. Fluids **55**, 1765 (2014).

[16]C. Y. Chen, C. Y. Lin, Y. T. Hu, L. Y. Cheng, and C. C. Hsu, Chem. Eng. J. **259**, 391–396 (2015).
[17]C. L. van Oosten, C. W. M. Bastiaansen, and D. J. Broer, Nat. Mater. **8**, 677–682 (2009).
[18]J. Dupire, M. Socol, and A. Viallat, Proc. Natl. Acad. Sci. U.S.A. **109**, 20808–20813 (2012).
[19]T. Omori, Y. Imai, K. Kikuchi, T. Ishikawa, and T. Yamaguchi, Ann. Biomed. Eng. **43**, 238–257 (2015).
[20]A. R. Pries and T. W. Secomb, Microcirculation **15**, 753–764 (2008).
[21]A. J. Mach and D. Di Carlo, Biotechnol. Bioeng. **107**, 302–311 (2010).
[22]S. Chien, Ann. Biomed. Eng. **36**, 554–562 (2008).
[23]C. Hahn and M. A. Schwartz, Nat. Rev. Mol. Cell Biol. **10**, 53–62 (2009).
[24]K. N. Dahl, A. Kalinowski, and K. Pekkan, Microcirculation **17**, 179–191 (2010).
[25]C. Y. Chen, M. J. Patrick, P. Corti, W. Kowalski, B. L. Roman, and K. Pekkan, Biorheology **48**(5), 305–321 (2011).
[26]T. L. Hedrick, Bioinspiration Biomimetics **3**, 034001 (2008).
[27]M. J. Patrick, C. Y. Chen, D. Frakes, O. Dur, and K. Pekkan, Exp. Fluids **50**, 887–904 (2011).
[28]See supplementary material at http://dx.doi.org/10.1063/1.4921427 for the demonstration of the time-reversible flow control with artificial cilia actuation.